10-1-2021

Behavioral and neurochemical studies of inherited manganese-induced dystonia-parkinsonism in Slc39a14-knockout mice

Alexander N. Rodichkin
Florida International University

Melissa K. Edler
Kent State University

Jennifer L. McGlothan
Florida International University

Tomás R. Guilarte
Florida International University

Neurobiology of Disease 158 (2021) 105467

Contents lists available at ScienceDirect

Neurobiology of Disease

journal homepage: www.elsevier.com/locate/ynbdi

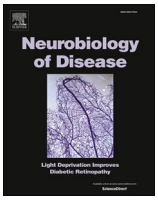

Behavioral and neurochemical studies of inherited manganese-induced dystonia-parkinsonism in *Slc39a14*-knockout mice

Alexander N. Rodichkin [a], Melissa K. Edler [b], Jennifer L. McGlothan [a], Tomás R. Guilarte [a,*]

[a] *Brain, Behavior, & the Environment Program, Department of Environmental Health Sciences, Robert Stempel College of Public Health & Social Work, Florida International University, Miami, FL 33199, United States of America*
[b] *Department of Anthropology and Brain Health Research Institute, Kent State University, Kent, OH 44242, United States of America*

ARTICLE INFO

Keywords:
Manganese
Dystonia-parkinsonism
Nigrostriatal dopaminergic system
Slc39a14 knockout mice

ABSTRACT

Inherited autosomal recessive mutations of the manganese (Mn) transporter gene *SLC39A14* in humans, results in elevated blood and brain Mn concentrations and childhood-onset dystonia-parkinsonism. The pathophysiology of this disease is unknown, but the nigrostriatal dopaminergic system of the basal ganglia has been implicated. Here, we describe pathophysiological studies in *Slc39a14*-knockout (KO) mice as a preclinical model of dystonia-parkinsonism in *SLC39A14* mutation carriers. Blood and brain metal concentrations in *Slc39a14*-KO mice exhibited a pattern similar to the human disease with highly elevated Mn concentrations. We observed an early-onset backward-walking behavior at postnatal day (PN) 21 which was also noted in PN60 *Slc39a14*-KO mice as well as dystonia-like movements. Locomotor activity and motor coordination were also impaired in *Slc39a14*-KO relative to wildtype (WT) mice. From a neurochemical perspective, striatal dopamine (DA) and metabolite concentrations and their ratio in *Slc39a14*-KO mice did not differ from WT. Striatal tyrosine hydroxylase (TH) immunohistochemistry did not change in *Slc39a14*-KO mice relative to WT. Unbiased stereological cell quantification of TH-positive and Nissl-stained estimated neuron number, neuron density, and soma volume in the substantia nigra pars compacta (SNc) was the same in *Slc39a14*-KO mice as in WT. However, we measured a marked inhibition (85–90%) of potassium-stimulated DA release in the striatum of *Slc39a14*-KO mice relative to WT. Our findings indicate that the dystonia-parkinsonism observed in this genetic animal model of the human disease is associated with a dysfunctional but structurally intact nigrostriatal dopaminergic system. The presynaptic deficit in DA release is unlikely to explain the totality of the behavioral phenotype and points to the involvement of other neuronal systems and brain regions in the pathophysiology of the disease.

1. Introduction

Manganese (Mn) is an essential trace element and required cofactor for many enzymes critical for human health (Aschner and Aschner, 2005). Since the early 1800s, occupational exposure to very high concentrations of Mn has provided evidence that when brain Mn concentrations increase significantly above physiological levels, Mn is neurotoxic and results in a neurological syndrome with early psychiatric symptoms followed by a form of parkinsonism with dystonia that is refractory to levodopa treatment, the pharmacotherapy used to control movement abnormalities in idiopathic Parkinson's disease (Couper, 1837; Guilarte, 2010; Guilarte, 2013; Guilarte and Gonzales, 2015; Blanc, 2018).

Historically, Mn-induced neurological disease has been most widely studied in occupationally exposed adult populations (Couper, 1837; Guilarte, 2010; Blanc, 2018). However, humans are exposed to Mn from a variety of occupational and environmental sources (Guilarte, 2010; Guilarte, 2013; Guilarte and Gonzales, 2015; Blanc, 2018), and recent cases of Mn-induced parkinsonism have been described in clinical populations. For nearly two decades, several reports have described young adult drug addicts exhibiting parkinsonism with dystonia as a result of injecting high Mn concentrations as a byproduct of the synthesis of the illicit psychostimulant drug ephedron (Meral et al., 2007; de Bie et al., 2007; Sanotsky et al., 2007; Sikk et al., 2007; Selikhova et al., 2008; Stepens et al., 2008; Colosimo and Guidi, 2009; Yildirim et al., 2009; Iqbal et al., 2012; Fudalej et al., 2013; Sikk et al., 2013;

* Corresponding author at: Robert Stempel College of Public Health & Social Work, Environmental Health Sciences, Cognitive Neuroscience & Imaging, Brain, Behavior & the Environment, Florida International University, 11200 SW 8th Street, Room AHC5-507, Miami, FL 33199, United States of America.
E-mail address: tguilart@fiu.edu (T.R. Guilarte).

https://doi.org/10.1016/j.nbd.2021.105467
Received 29 March 2021; Received in revised form 14 July 2021; Accepted 2 August 2021
Available online 4 August 2021

Poniatowska et al., 2014; Janocha-Litwin et al., 2015; Sikk et al., 2010). More recently, childhood-onset dystonia-parkinsonism with increased blood and brain Mn concentrations has also been described in individuals with inherited autosomal recessive mutations of the Mn transporter genes *SLC30A10* (Gospe et al., 2000; Sahni et al., 2007; Tuschl et al., 2008; Brna et al., 2011; Quadri et al., 2012; Stamelou et al., 2012; Tuschl et al., 2012; Lechpammer et al., 2014) and *SLC39A14* (Tuschl et al., 2016; Juneja et al., 2018; Marti-Sanchez et al., 2018; Rodan et al., 2018; Zeglam et al., 2019). These genetic mutations produce dysfunction of Mn transporters leading to highly elevated Mn concentrations in the blood and brain and clinical expression of childhood-onset dystonia-parkinsonism. One important aspect of this population of Mn transporter mutation carriers is that the chronic Mn exposure occurs when the brain is developing in contrast to adult Mn exposures in the case of occupational and ephedron addicts in which the exposures typically occur when the brain is fully developed. Therefore, it is possible that neuronal systems and brain regions are differentially affected based on the age when the high Mn exposure occurs in the brain.

Nevertheless, the discovery of inherited autosomal recessive mutations of the Mn transporter genes *SLC30A10* and *SLC39A14* has revolutionized the study of Mn homeostasis and neurotoxicity (Mukhopadhyay, 2018). These genes code for critical Mn transporters that are involved in the efflux (*SLC30A10*) and influx (*SLC39A14*) of Mn in cells to maintain Mn homeostasis. Clinical populations have significantly advanced our understanding of Mn homeostasis and Mn-induced neurological disease in that these Mn transporters work in concert to excrete Mn from the body and disruption of this fine balance results in systemic Mn retention and highly increased concentrations of Mn in the brain (Mukhopadhyay, 2018). Despite these important findings, there is a paucity of knowledge on the neuronal systems and brain regions affected in the inherited mutation carriers, and there is a lack of comprehensive neuropathological studies in humans with the disease and in preclinical animal models in order to understand the pathophysiology of childhood-onset dystonia-parkinsonism of *SLC39A14* mutation carriers.

While significant research in experimental animal models, and more limited studies in humans, has been described with adult-onset Mn-induced parkinsonism and its effects on the nigrostriatal dopaminergic system (Couper, 1837; Guilarte, 2010; Guilarte, 2013; Guilarte and Gonzales, 2015; Blanc, 2018), less is known about the effects of chronically elevated blood and brain Mn concentrations during early life as is the case with individuals expressing the autosomal recessive mutations of the *SLC39A14* and *SLC30A10* genes. However, one of the most consistent changes in brain chemistry with Mn exposure in adult animals is the inhibition of dopamine (DA) release (Guilarte et al., 2006; Guilarte et al., 2008; Guilarte et al., 2019; Khalid et al., 2011). We have previously shown that non-human primates chronically exposed to Mn as young adults with subtle motor function deficits have significant impairment of *in vivo* amphetamine-induced DA release in the caudate/putamen measured using positron emission tomography (PET) (Guilarte et al., 2006; Guilarte et al., 2008) as well as in the frontal cortex (Guilarte et al., 2019). Similarly, rodents exposed to Mn as adults also have inhibition of potassium-stimulated DA release in the striatum (Khalid et al., 2011). Therefore, inhibition of striatal DA release whether stimulated by amphetamine or potassium depolarization is a consistent observation on the effects of chronic adult Mn exposure on DAergic circuits in experimental animal models.

The recent availability of *Slc30a10* and *Slc39a14* global knockout (KO) mice provide a genetic-based approach to study Mn-induced neurological dysfunction and underlying neuropathology. Previous studies have shown that *Slc39a14*-KO mice exhibit increased blood and brain Mn concentrations as well as motor function deficits and postural and gait abnormalities as in the human *SLC39A14* mutation carriers (Aydemir et al., 2017; Xin et al., 2017; Jenkitkasemwong et al., 2018). Notably, *Slc39a14*-KO mice from a B6:129 hybrid background were backcrossed onto a 129S6/SvEvTac strain, similar blood and brain increases in Mn concentrations were obtained (Jenkitkasemwong et al., 2018) indicating that the deletion of *Slc39a14* results in increased blood and brain Mn concentrations despite the genetic background of the mice and increased brain Mn may be responsible for the behavioral changes observed (Jenkitkasemwong et al., 2018). However, no study to date has described the neurochemical or neuropathological bases of the Mn-induced dystonia-parkinsonism in mice with genetic deletion of these Mn transporters. In the present work, we used *Slc39a14*-KO mice to assess the behavioral, neurochemical, and neuropathology of the nigrostriatal dopaminergic system resulting from increased brain Mn concentrations in young adult male and female mice. The nigrostriatal dopaminergic system of the basal ganglia was initially selected because it has been implicated in Mn-induced parkinsonism with dystonia (Guilarte, 2010; Guilarte, 2013; Guilarte and Gonzales, 2015; Guilarte et al., 2006; Guilarte et al., 2008) and in different dystonia animal models (Balcioglu et al., 2007; Hewett et al., 2010; Song et al., 2012; Ip et al., n.d.; Eskow Jaunarajs et al., 2019; Rauschenberger et al., 2020).

2. Materials and methods

2.1. Animal husbandry and genotyping

Animal studies were reviewed and approved by the Florida International University Animal Care and Use Committee, comply with the ARRIVE guidelines, and were carried out in accordance with the National Institutes of Health Guide for the Care and Use of Laboratory Animals. The *Slc39a14*-KO founder mice were generously provided by Dr. Robert J. Cousins from the University of Florida, where the colony was originally described (Aydemir et al., 2012). Briefly and as described in the original publication (Aydemir et al., 2012), Zip14 +/− and Zip14 +/+ founder mice were obtained through a contract with the Mutant Mouse Regional Resource Center at the University of California, Davis. A targeted mutation in Zip14 gene (exons 3–5) was generated in strain 129/SvEvBrd derived embryonic stem cells. The chimeric mice were bred to C57BL/6 J albino mice to generate Zip14 +/− mice. Zip14 −/− mice were obtained through further breeding of founder Zip14 +/− mice at the University of Florida (Aydemir et al., 2012). Animals were bred using 1:1 male:female Zip14 +/− mice generating Zip14 +/+ (*Slc39a14-WT) and Zip14 −/− (Slc39a14-KO) mice for the studies.* Litters were weaned at post-natal day (PN) 21. Animals were housed on a 12:12 light:dark cycle with *ad-libitum* food and water access. The rodent chow was Advanced Protocol Verified 75 IF irradiated 5 V75* diet (Lab diets, Ft. Worth, Texas). ICP-MS analysis of Mn, iron, copper, and zinc of this rodent chow indicated the following concentrations: Mn = 110.5 ± 15.7 μg/g; Iron = 163.1 ± 27.8 μg/g; Copper = 10.7 ± 2.2 μg/g, and Zinc = 79.6 ± 14.5 μg/g. All values are mean ± sem of 5 different samples.

For genotyping, a tail clip was taken immediately after weaning using a pair of sterilized scissors. DNA extraction solution (200 μL) was added to the homogenized tissue samples (QuickExtract DNA Extraction Solution 1.0, Lucigen, Middleton, WI) and heated to 65°C for 6 min and 95°C for 2 min. A Verti Applied Biosystems Thermocycler (ThermoFisher Scientific, Waltham, MA) was used for the PCR reaction under the following conditions: 1) 95°C for 5 min, 2) 95°C for 30s, 53°C for 30s and 72°C for 1 min for 35 cycles, 3) 72°C for 10 min. The following primer sequences were used: *Slc39a14*-WT forward: 5′ – TCA TGG ACC GCT ATG GAA AG – 3′; *Slc39a14*-WT reverse: 5′ – GTG TCC AGC GGT ATC AAC AGA GAG – 3′; *Slc39a14*-KO forward: 5′ – TGC CTG GCA CAT AGA AAT GC – 3′; *Slc39a14*-KO reverse: 5′ – GCA GCG CAT CGC CTT CTA TC – 3′. PCR products were run through 1.5% agarose gel made in 1xTAE buffer containing Gel Red stain (3.75 μL of Gel Red in 100 mL agarose; Biotum, Fremont, CA) at 120 V for 90 min with *Slc39a14*-WT band at 164 bp and *Slc39a14*-KO band at 469 bp [see example of gel genotyping Supplementary Fig. 1].

2.2. Metal analysis

Brain tissue and whole blood specimens for metals analyses were obtained from animals that were used in behavioral assessments. Tissue metals concentrations were corrected for wet tissue weight. *Blood metals:* Whole blood was obtained immediately following decapitations and collected directly into K_2EDTA coated tubes (BD Vacutainer, Becton Dickinson and Company, Franklin Lakes, NJ). 100 μL of whole blood was mixed with 250 μL tetramethylammonium hydroxide (TMAH) solution and allowed to incubate for 10 min at room temperature (RT). Afterwards, 50 μL of internal standards (IS) mixture containing lithium, yttrium and germanium was added. A 0.005% EDTA and 0.005% Triton-X solution made in ultra-pure water was used to bring the total volume to 5 mL, resulting in final IS concentration of 10 μg/L. The samples were then placed into the autosampler (CETAC-ASX 520, ThermoFisher Scientific, Waltham, MA) and directly injected into the ICP-MS (iCAP-TQ, ThermoFisher Scientific, Waltham, MA) using the S-SQ-KED High Sensitivity detection mode. Qtegra Software (ThermoFisher Scientific, Waltham, MA) was used to construct the calibration curves and perform the analysis (Nunes et al., 2010). *Striatum metals*: Striatal punches were taken from flash frozen tissue slabs obtained after euthanizing of mice. Tissue punches were weighed and stored at -80°C until analysis. Samples were mixed with 1 mL of concentrated HNO_3 and allowed to digest for 2 h at 95°C in a heating block. After digestion, samples were allowed to cool down to RT and 100 μL of IS mixture containing lithium, yttrium and germanium was added. Total volume was brought up to 10 mL using 3% HNO_3 made in ultra-pure water, resulting in final IS concentration of 10 μg/L. Both blood and brain samples and calibration curve solutions were processed into the autosampler and injected into the ICP-MS using S-SQ-KED High Sensitivity detection mode. Qtegra Software was used to construct the calibration curves and perform the analysis.

2.3. Behavioral assessment

All behavioral tests were performed between 12:00 and 18:00 h, during the light cycle, with the exception of locomotor activity, that was performed in the dark cycle. Separate naïve animals were used for each test, with 1 male or female animal per litter used for each endpoint. *Activity cages:* For locomotor activity recordings, naïve animals were habituated to the behavior room for 30 min. Animals were placed into the activity cages (Activity Cages Monitor SOF-812, Med Associates, Fairfax, VT) for 60 min. All locomotor activity recordings were performed after 19:00 h, during the dark cycle. *Rotarod:* Rotarod testing took place over the course of 3 days. In the beginning of each day, the animals were habituated to the testing room for 10 min. Following the habituation period, they were trained on the rotarod (Columbus Instruments, Columbus, OH) for 5 min at 4RPM and then allowed to rest in their home cage for 30 min. After the resting period concluded, animals were placed on the rotarod, starting at 4RPM and accelerating by 4 RPM every 30 s for 3 trials per day. Latency-to-fall was recorded and values from 3 trials were averaged (Loth et al., 2016). *Behavioral observations for dystonia features using the tail suspension test*: We performed the tail suspension test and observed for dystonia-like features as described in previous studies (Eskow Jaunarajs et al., 2019; Liang et al., 2014; Xiao et al., 2020). The animal was gently and carefully suspended by the end of the tail 20 cm from the bottom of the cage for the duration of 1 min and recorded on video. A blinded investigator unfamiliar with the animals analyzed the videos, screening for the following behaviors: front limb clasping, hind limb clasping, truncal torsion, cervical torsion, splaying of the toes, unilateral use of limbs and decreased movement. At PN21, we also observed for torticollis, retrocollis, straub tail, backward walking, foot dragging and splayed paws from videos of *Slc39a14*-KO mice compared to WT. The number of *Slc39a14*-KO mice expressing these abnormal behaviors is provided in supplementary Table 1.

2.4. Analysis of dopamine and metabolites concentrations in the corpus striatum

Tissue punches of the striatum were obtained at the level of the lateral ventricles [AP: 0.14 DV: -3.5 ML: 2.0] from brains of WT and *Slc39a14*-KO mice, and the tissue immediately frozen at -80°C until analysis. On the day of the analysis, sample weights were recorded, the tissue was placed into 30× *w/v* 0.1 M perchloric acid and went through 3 cycles of sonication 10s-on/10s-off (Tekmar Sonic Disruptor, Teledyne Tekmar Company, Inc., Mason, OH) while on ice. The resulting solution was filtered using PTFE-membrane 20 μm centrifugal tubes (Ultrafree-MC Centrifugal Devices, Millipore-Sigma, Burlington, MA; 4°C, 15,000 g, 15 min). The protein pellet was frozen at -80°C until analysis. The resulting supernatant was diluted in 0.1 M perchloric acid at a 1:3 ratio and 10 μL were injected into the HPLC-ECD (Dionex Ultimate 3000, ThermoFisher Scientific, Waltham, MA) using the MDTM mobile phase, reverse phase column (C18-Hypersil 150 mm × 2.1 with 3 μm particle size, ThermoFisher Scientific, Waltham, MA) and amperometric cell (Dionex Ultimate 3000 ECD-3000RS Electrochemical Detector, ThermoFisher Scientific, Waltham, MA) set at +400 mV, 10 nA gain with 0.4 mL/min flow rate. 50 ng/mL 2,5-dihydroxybemzoic acid was used as the internal standard (Yang and Beal, 2011). The recovered protein pellets were analyzed using the commercially available BCA assay (Pierce BCA Protein Assay Kit, ThermoFisher Scientific, Waltham, MA). Dopamine and metabolite concentrations were normalized with protein concentrations.

2.5. Tyrosine hydroxylase (TH) immunohistochemistry

Animals were perfused using 4% paraformaldehyde (PFA) solution made in 0.1 M phosphate buffer. The extracted tissue was suspended in 4% PFA for 24 h and cryoprotected in 30% sucrose solution for 48 h. Snap-frozen brains were sectioned at 40 μm (American Optical Company Microtome, Model 860) with sections placed in individual wells containing freezing storage solution (30% glycerol, 30% ethylene glycol, 30% dH_2O and 10% 0.24 M phosphate buffer). Every third section throughout the substantia nigra pars compacta (SNc) was stained for TH, the rate-limiting enzyme for DA synthesis, and used for unbiased stereological cell counting. For TH optical density in the striatum, every sixth section was used. The sections were washed in a 1× phosphate-buffer saline solution (PBS, pH 7.4) at RT. Antigen retrieval was performed using 10 mM sodium citrate buffer at 37 °C for 30 min, followed by a 20 min incubation at RT. Endogenous peroxidase was quenched in 2.5% hydrogen peroxide (H_2O_2) made in 75% methanol solution for 20 min at RT. Tissue sections were pre-blocked using 0.6% Triton X-100, 5% bovine serum albumin, and 4% normal horse serum (S-2000, Vector Laboratories, Burlingame, CA) for 1 h at RT. Tissue was incubated in a 1:10,000 primary antibody (anti-tyrosine hydroxylase monoclonal antibody, MAB-318, clone LNC1, Millipore-Sigma, Burlington, MA) overnight at RT. On the following day, the tissue was placed in a biotinylated secondary antibody solution (1:200, BA-2000, Vector Laboratories, Burlingame, CA), containing 2% normal horse serum for 1 h at RT. The tissue was then incubated for 1 h at RT in Avidin-biotin-peroxidase complex (ABC kit, PK-6100, Vector Laboratories, Burlingame, CA) followed by development in 3,3′-diaminobenzidine for 10 min at RT (DAB kit, SK-4100, Vector Laboratories, Burlingame, CA). Sections were mounted on slides, dehydrated in a series of ethanol solutions and cover slipped using the EMS-DPS mounting medium.

2.6. Unbiased stereology of TH and Nissl estimated neuron number, neuron density (Nv), and soma volume (SV)

Using the Allen mouse coronal brain atlas (Allen Atlas for Brain Science), we measured TH-positive and Nissl estimated neuron number, Nv and SV in the SNc of PN60 male and female wildtype ($n = 12$: 6 male, 6 female) and *Slc39a14*-KO (n = 12: 6 male, 6 female) mice. All data

were collected using StereoInvestigator software (Version 11.11.2, MBF Bioscience, Williston, VT, RRID:SCR_002526) and an Olympus BX-51 photomicroscope (Olympus, Center Valley, PA) equipped with a digital camera by a single, blinded observer. Initial subsampling techniques were performed to determine appropriate sampling parameters (Slomianka and West, 2005). Beginning at a random starting point, TH-positive and Nissl Nv (mm^3) were obtained using the optical dissector probe at 40× (N.A. 0.75) under Köhler illumination. Six equidistant sections (1:3 series) throughout the SNc were selected for TH Nv quantification, while 3–4 sections were used to collect Nissl Nv (1:6 series). TH-positive and Nissl neurons were designated with a single marker per stain, and sampling area size was 100 × 100 with a dissector height of 7 μm and a guard zone of 2%. Mounted section thickness was measured every fifth sampling site. Densities (i.e., Nv) were calculated as the estimated neuron population of TH- or Nissl-positive markers divided by planimetric volume of the dissector for each area of interest and averaged for every animal (Sherwood et al., 2005). SV was collected for every TH-positive neuron and every fourth Nissl-stained neuron using the isotropic nucleator simultaneously during the optical fractionator probe. Six rays were used to define the soma edge. The average measured thickness for TH-stained sections was 19.49 μm and for Nissl sections was 13.00 μm, and the mean number of sampling sites for TH was 169 ± 39 and for Nissl was 56 ± 5 with a Gunderson coefficient of error (CE) of 0.06. The mean number of nucleators for TH was 121 and for Nissl was 86 with average CEs ≤ 0.01 for SV.

2.7. In vivo microdialysis and HPLC analysis of dopamine and metabolites in dialysates: Cannulations

Animals were anesthetized with an intraperitoneal injection of ketamine (100 mg/kg) and xylazine (10 mg/kg). Once the animals no longer responded to paw pinches and blinking reflexes were not observed, animals were administered atropine (5 mg/kg, subcutaneous). A small amount of betadine was used to prepare the incision site. Following betadine application, a 100 μL injection of lidocaine was made in the same location. A pre-sterilized scalpel blade was used to make an incision in the scalp, approximately 2 cm along the sagittal suture, exposing the skull. Following the incision, the mouse was placed into the stereotaxic frame (Neurostar, Tubingen,Germany) and eye ointment was applied. The coordinates for the guide cannula placement (MBR-5 5 mm guide cannula, BASi, West Lafayette, IN) were AP: +1.18, ML: +1.5, and DV: −2.4 (Paxinos and Franklin, 2001), and the cannula implant was secured with small anchor screws set into the skull (self-tapping bone anchor screws, BASi, West Lafayette, IN). Loctite-444 was used to bind the cannula and screws together with the bone. Upon successful cannulation, animals were administered yohimbine (2 mg/kg) and meloxicam (5 mg/kg) and monitored until voluntary movement appeared. Prior to *in vivo* microdialysis, animals went through a 3-day recovery period with daily administrations of meloxicam (5 mg/kg). Workup, cannulations, and recovery were all completed on heating pads.

2.8. In vivo microdialysis

Animals were habituated to the room for 30 min. Immediately before the procedure, animals were fitted with collars and the dummy probe was removed from the guide cannula and replaced with the actual probe (MBR 1–5, 1 mm probe, BASi, West Lafayette, IN). Animals then were connected to microdialysis tubing and the Raturn system *via* the collar and artificial CNS fluid (NaCl 147 mmol/L, KCl 2.7 mmol/L, $CaCl_2$ 1.2 mmol/L, $MgCl_2$ 0.85 mmol/L, Harvard Apparatus, Holliston, MA) was perfused for an equilibration period of 3 h at 1 μL/min. Following the equilibration period, 15 samples in 20-min intervals were collected at 1 μL/min (BAS Honeycomb refrigerated fraction collector, BASi, West Lafayette, IN) into 300 μL limited volume inserts containing 2 μL of 0.1 M perchloric acid, resulting in 22 μL final volume per sample. Immediately after collection, each sample was transferred to the HPLC-ECD system for injection and analysis, using the same parameters as the analysis for striatal dopamine concentrations (Yang and Beal, 2011). Neuronal depolarization in the target region was achieved by switching the perfusion fluid to 120 mM KCl solution (made in aCNS fluid) for a 20-min per sample period during the 5th sample collection phase. *In vivo* microdialysis was performed during the night cycle with pairs of WT and KO animals being sampled at the same time side-by-side with the same solutions. Verification of dialysis probe location in the striatum was performed using Nissl staining and the findings are provided in Supplementary Fig. 2.

2.9. Statistical analysis

Stereologic data analysis was performed using unpaired *t*-tests comparing the means of WT versus *Slc39a14*-KO mice. Rotarod data were analyzed using a two-way repeated measures ANOVA. Prior to analyses, data were examined for outliers using the ROUT method (Q = 1). In addition, tests for equality of variance (F-test) and normality of residuals were performed. Statistical analyses were completed using GraphPad PRISM (Version 8.4.0 (455), La Jolla, CA), and α was set at 0.05.

3. Results

3.1. Body and brain weight of WT and Slc39a14-KO mice

Most of the studies were performed in WT and *Slc39a14*-KO mice at PN60. However, body weights were recorded at PN30, PN45, and PN60 (Supplementary Fig. 3). Analysis of variance indicates that there was no significant effect of genotype on body weight of male ($F_{1,15} = 0.910$, $p = 0.36$) or female mice ($F_{1,15} = 0.286$, $p = 0.60$). At PN60, when animals were euthanized, whole brain weight (frozen) was measured with no significant effect of genotype in male and female mice brain weight (Supplementary Fig. 3).

3.2. Blood and brain metals concentrations

We measured the concentrations of Mn, copper, iron, and zinc in whole blood samples from WT and *Slc39a14*-KO male and female mice at PN60. Highly significant increases in blood Mn concentrations were found in both male (Fig. 1A) and female (Fig. 1B) *Slc39a14*-KO mice relative to WT. On the other hand, no differences were identified in iron, copper, or zinc concentrations in the blood of male (Fig. 1A) or female (Fig. 1B) *Slc39a14*-KO relative to WT at this age. This is consistent with what was found in the *SLC39A14* mutation carriers (Tuschl et al., 2016). We also measured metal concentrations in the striatum, as this brain region is associated with movement abnormalities and is implicated in dystonia-parkinsonism. Fig. 1 shows that Mn concentrations in the striatum of PN60 *Slc39a14*-KO was approximately 5 times higher than WT in both male (Fig. 1C) and female (Fig. 1D) mice. No significant effect was determined for genotype on iron, copper, or zinc concentrations in the striatum of male (Fig. 1C) or female (Fig. 1D) mice at this age.

3.3. Behavioral studies

To assess the effect of the *Slc39a14* deletion on locomotor activity, motor coordination, and dystonia-like movements, we performed a variety of behavioral and observational studies on male and female PN21 (weaning) and PN60 mice.

3.3.1. Locomotor activity

Locomotor activity was assessed during the dark cycle using automated activity cages at PN60. Significant impairment of locomotor activity was demonstrated in both male (Fig. 2B) and female (Fig. 2C)

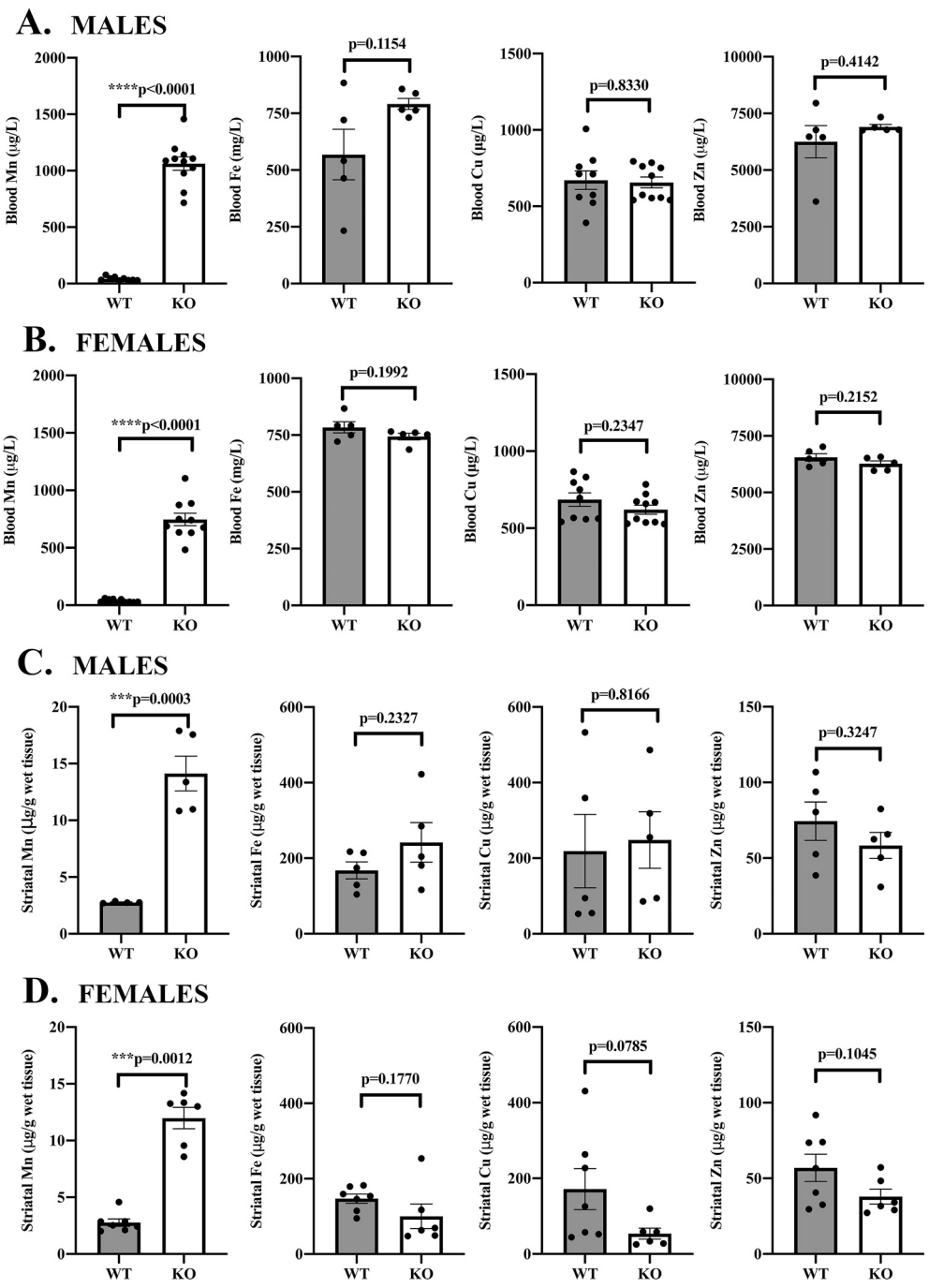

Fig. 1. Blood and brain metals concentrations in WT and *Slc39a14*-KO PN60 mice: A) Whole blood concentrations of manganese, iron, copper, and zinc in male WT and KO mice. *Slc39a14*-KO mice exhibited highly significant ($p < 0.0001$) increases in blood Mn levels with no effect on other metals concentrations. ($n = 5–11$) B) Similarly, female *Slc39a14*-KO mice also expressed significantly ($p < 0.0001$) increased blood Mn concentrations with no effect on the concentrations of other metals. (n = 5–10) C) Concentrations of manganese, iron, copper, and zinc in the striatum of *Slc39a14*-KO and WT male mice. There was a significant increase in striatal Mn concentrations ($p = 0.0003$) with no effect on other metals. ($n = 4–5$) D) A similar increase ($p = 0.0012$) was measured in the concentration of Mn in the striatum of female mice with no effect on other metals. (n = 5–7) Values are mean ± SEM.

Slc39a14-KO mice relative to WT. Male (Fig. 2B) and female (Fig. 2C) PN60 *Slc39a14*-KO mice had significantly decreased distance traveled, speed, and vertical counts (rearing), with an increase in resting time, consistent with a significant impairment in locomotor behavior.

3.3.2. Rotarod measurements

Rotarod analysis examined the effect of global *Slc39a14* deletion and resulting increased brain Mn concentrations on motor coordination and motor skill learning. Both male (Fig. 2D) and female (Fig. 2E) *Slc39a14*-KO mice experienced a significant impairment relative to WT. For example, the latency to fall from the turning rod decreased for all 3 days in *Slc39a14*-KO mice compared to WT. Combined, the locomotor and rotarod results clearly indicate significant impairment of normal motor function and coordination in the PN60 *Slc39a14*-KO male and female mice relative to WT.

3.3.3. Observational studies of dystonia-like movements and ataxia (video and pictures)

We observed abnormal locomotor behavior in some of the *Slc39a14*-KO mice at weaning (PN21). That is, *Slc39a14*-KO mice express backward walking behavior (see Supplementary Movie 1) at weaning with a wider separation of the hindlimbs and a shuffling gait. To our knowledge, this type of backward walking behavior has only been previously observed in moonwalker mice (Becker et al., 2009). Further, when *Slc39a14*-KO mice attempted to move forward, dragging of the hind limb was noted in some animals (see Supplementary Movie 2). The backwards movement in the *Slc39a14*-KO was also observed in *Slc39a14*-KO mice at PN60. A portion of *Slc39a14*-KO mice had tilting of

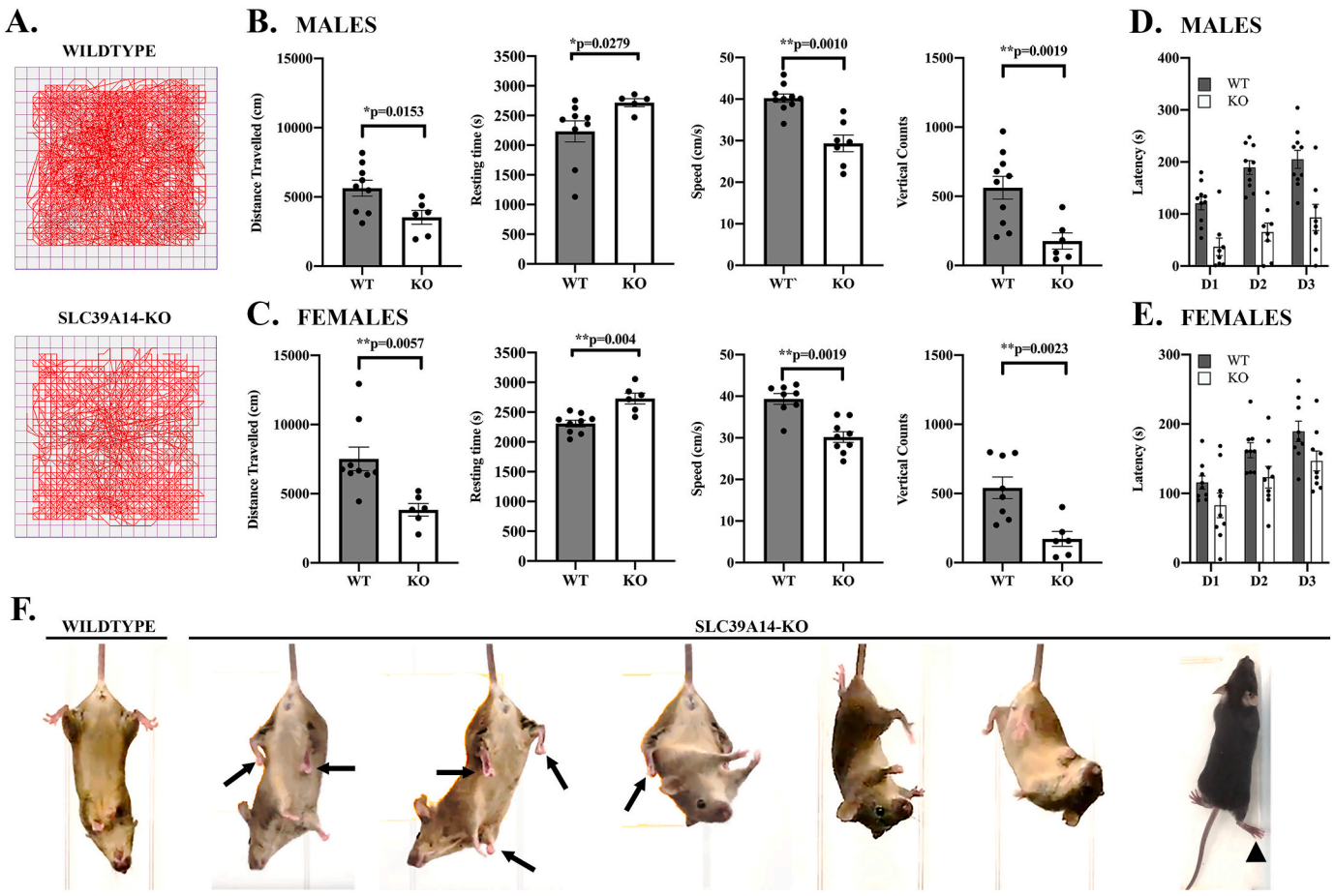

Fig. 2. Behavioral assessment of WT and *Slc39a14*-KO PN60 mice: A) Representative examples of activity cage tracking of the movement of WT and KO mice. B) Analysis of locomotor behavior using activity cages in WT and *Slc39a14*-KO male mice at PN60. There were highly significant effects on the *Slc39a14*-KO mice on distance traveled (decreased, $p = 0.0153$), resting time (increased, $p = 0.0279$), speed (decreased, $p = 0.001$), and vertical counts (decreased, $p = 0.0019$). ($n = 5$–9) C) Locomotor behavior of WT and *Slc39a14*-KO female mice. Similar to the male mice, female *Slc39a14*-KO mice also expressed a decrease in distance traveled ($p = 0.0057$), increase in resting time ($p = 0004$), decrease in speed (p = 0.0019), and decrease in vertical counts ($p = 0.0023$). ($n = 6$–9) D) Rotarod performance of WT and *Slc39a14*-KO male mice shows a significant genotype effect [$F_{1,12} = 14.7$; $p = 0.0001$] indicating that in *Slc39a14*-KO, the latency to fall from the rotating cylinder was significantly shorter than WT mice. (n = 6–10) E) Rotarod performance of WT and *Slc39a14*-KO female mice also show a significant genotype effect [$F_{1,16} = 5.08$; $p = 0.0398$ ($n = 9$)]. F) Observational studies of dystonia features in *Slc39a14*-KO mice using a tail suspension test. We observed dystonia-like movements in the *Slc39a14*-KO mice including trunk twisting, hindlimb clasping, and dragging of the foot while forward walking. Also, we observed backward walking behavior of *Slc39a14*-KO mice at PN21 (see Supplementary Movie 1). Values are mean ± SEM.

the head to the left side (torticollis) and back (retrocollis), and straub tail (Supplementary Table 1). Using the tail suspension test, we showed that *Slc39a14*-KO mice expressed dystonia-like movements such as trunk twisting and hind limb clasping a greater percentage of the time than WT (Fig. 2F and Supplementary Table 1).

3.4. Neurochemical and neuropathological assessment of nigrostriatal dopaminergic system

The motor function deficits of the *Slc39a14*-KO mice could be the result of dysfunction or degeneration of the nigrostriatal dopaminergic system as DA neurons of the SNc have been implicated in a variety of movement disorders including dystonia and parkinsonism with idiopathic Parkinson's disease being the most prominent form of parkinsonism. Therefore, we performed an assessment of nigrostriatal dopaminergic markers in PN60 WT and *Slc39a14*-KO mice.

3.4.1. Analysis of dopamine and metabolite concentrations in the striatum

We performed HPLC-electrochemical detection of DA and its metabolites 3,4-dihydroxyphenylacetic acid (DOPAC) and homovanillic acid (HVA) as well as metabolite to DA ratios in the striatum of male and female WT and *Slc39a14*-KO mice at PN60. Global deletion of the *Slc39a14* gene which produces increased blood and brain Mn concentrations and motor function deficits had no significant effect on striatal DA concentrations or in the concentrations of the DA metabolites DOPAC or HVA in male (Fig. 3A) or female (Fig. 3B) *Slc39a14*-KO mice compared to WT. Furthermore, the ratios of DOPAC/DA and HVA/DA which are measures of DA turnover also were not significantly affected in *Slc39a14*-KO mice of either sex (Fig. 3A-B).

3.4.2. Tyrosine hydroxylase (TH) immunohistochemistry and optical density analysis of nigrostriatal dopaminergic neuron terminals in the striatum

To determine if there was an effect on nigrostriatal dopaminergic terminals in the striatum, we performed TH immunohistochemistry in the striatum of WT and *Slc39a14*-KO mice. Optical density measures demonstrated no differences in the level of TH immunoreactivity by genotype (Fig. 3C-E). These findings indicate that nigrostriatal dopaminergic terminals in the striatum of *Slc39a14*-KO mice are intact, despite highly increased brain Mn concentrations and deficits in motor function.

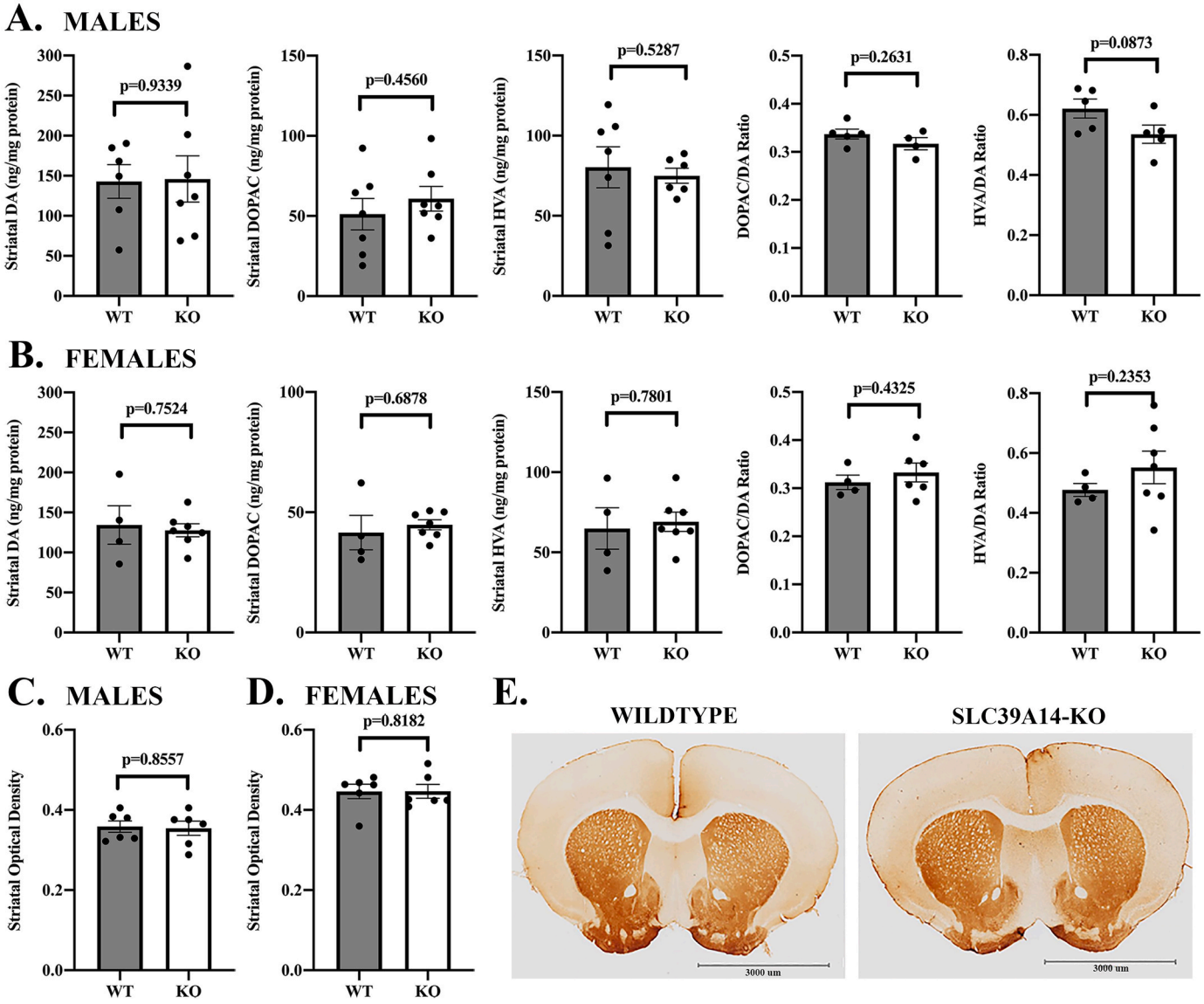

Fig. 3. Analysis of the nigrostriatal dopaminergic system in WT and *Slc39a14*-KO PN60 mice in the corpus striatum: (A,B) HPLC-electrochemical detection of DA, DOPAC, HVA, DOPAC/DA, and HVA/DA in the striatum of PN60 WT and *Slc39a14*-KO male (A) and (B) female mice. No significant differences were found in any of the measurements in either sex. (n = 4–7) (C,D) Tyrosine hydroxylase (TH) immunostaining optical density in the striatum of male (C) and female (D) WT and *Slc39a14*-KO mice. (n = 6) E) representative images of TH immunohistochemistry in the striatum of WT and *Slc39a14*-KO mice. No significant differences were found in any of the measurements in either sex. Values are mean ± SEM.

3.4.3. TH and Nissl Nv and SV in the SNc

To further assess the integrity of nigrostriatal DAergic neurons, we performed unbiased stereological quantification of TH Nv and SV in the SNc. TH Nv and Sv did not differ in the SNc of WT and *Slc39a14*-KO male (Fig. 4A, C) and female (Fig. 4B, D) mice. To confirm the lack of an effect resulting from the *Slc39a14* gene deletion on overall Nv and Sv, we also analyzed Nissl Nv and SV in the SNc. Consistent with TH Nv and SV, there were no differences in Nissl Nv or SV between *Slc39a14*-KO mice and WT male or female mice (Supplementary Fig. 4). In order to obtain Nv, for either TH or Nissl neurons in the SNc, the average estimated number of neurons was divided by the average planimetric volume. Analysis of the average estimated number of TH-positive or Nissl-stained neurons also shows no significant differences between WT and *Slc39a14*-KO mice of either sex (Supplementary Table 2).

3.4.4. In vivo microdialysis of basal and potassium-stimulated dopamine release in the striatum

Previous work from our laboratory on the effects of chronic Mn exposure in young adult non-human primates showed that a prominent effect of chronic Mn exposure on the nigrostriatal dopaminergic system was marked inhibition of amphetamine-induced DA release in the caudate/putamen (striatum) measured by PET (Guilarte et al., 2006; Guilarte et al., 2008). This effect of chronic Mn exposure has also been shown in adult mice chronically exposed to Mn (Khalid et al., 2011). In this rodent study, striatal DA release was stimulated using high potassium concentrations. Therefore, we measured the basal and potassium-stimulated release of DA in the striatum using *in vivo* microdialysis. We found a marked inhibition (85–90%) of potassium-stimulated DA release in PN60 *Slc39a14*-KO male (Fig. 5C) and female (Fig. 5D) mice relative to WT consistent with previous Mn-exposed non-human primate (Guilarte et al., 2006; Guilarte et al., 2008) and in rodents (Khalid et al., 2011).

4. Discussion

To our knowledge, this is the first report describing neurochemical

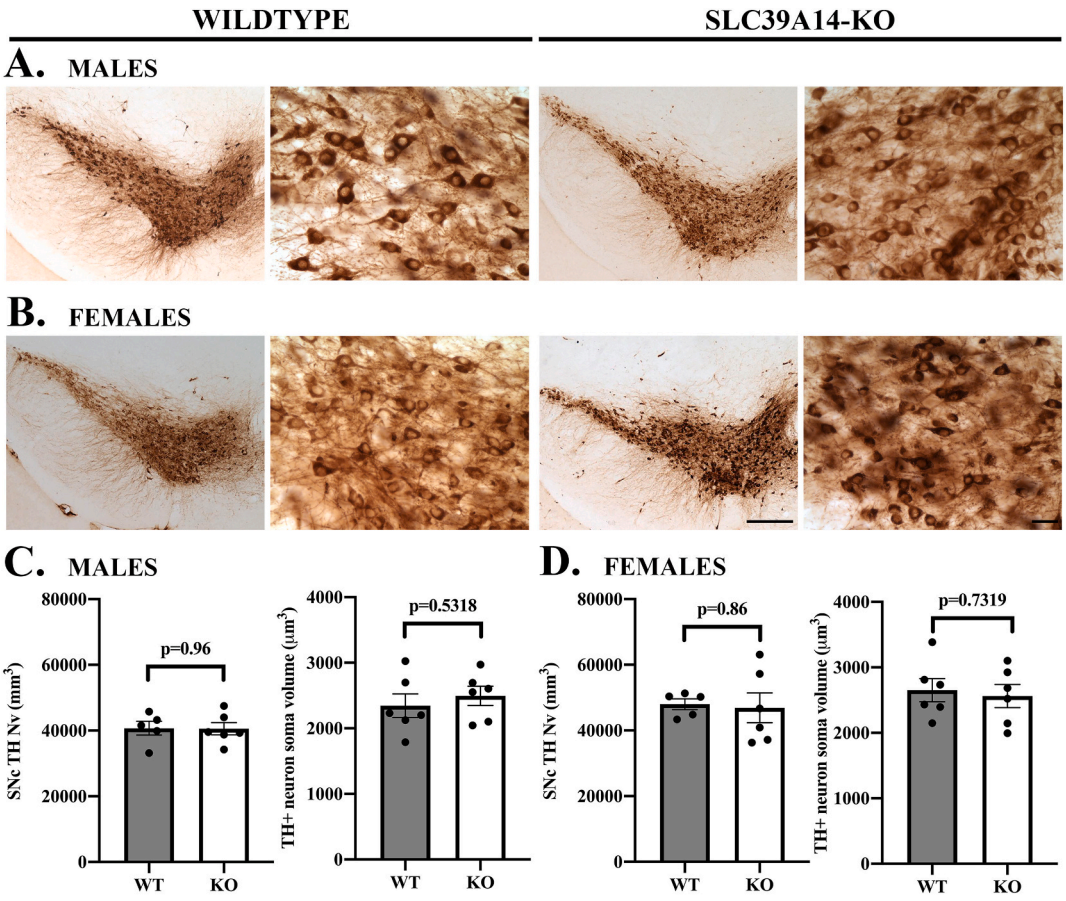

Fig. 4. Unbiased stereological counting of TH neuron density (Nv) and soma volume (SV) in the SNc of WT and *Slc39a14*-KO PN60 mice: Photomicrographs of TH immunoreactivity in the SNc of PN60 male (A) and female (B) WT and KO mice. Scale bars = 250 µm (low magnification) or 25 µm (high magnification). There were no significant differences inNv or SV in the *Slc39a14*-KO male (C) or female (D) mice relative to WT. Average SNc TH Nv was 40,324/mm^3 in male WT mice ($n = 5$), 40,561/mm^3 in male *Slc39a14*-KO mice ($n = 6$), 48,012/mm^3 in female WT mice (n = 5), and 46,913/mm^3 in female *Slc39a14*-KO mice (n = 6). Importantly, SNc TH Nv did not differ between male ($t_{10} = 0.06$, $R^2 = 0.00$, $p = 0.96$) or female ($t_{10} = 0.21$, $R^2 = 0.00$, $p = 0.84$) WT and *Slc39a14*-KO mice. Values are mean ± SEM.

changes of the nigrostriatal dopaminergic system associated with the motor function deficits, postural and gait abnormalities in *Slc39a14*-KO mice, a preclinical model of the childhood-onset dystonia-parkinsonism resulting from the inherited autosomal recessive mutations of the *SLC39A14* gene in humans. As outlined by Tuschl et al., (Tuschl et al., 2016) in their original communication describing individuals expressing this inherited mutation, there are similarities in the behavioral deficits in *Slc39a14*-KO mice as in the human disease. For instance, affected individuals experience an early loss of developmental milestones, progressive dystonia, and bulbar dysfunction. They later develop severe generalized and pharmaco-resistant dystonia, spasticity, scoliosis, and loss of independent ambulation. In some cases, there was parkinsonism with hypomimia, tremor, and bradykinesia. From a neuroimaging perspective, the *SLC39A14* mutation carriers exhibited hyperintensive signals based on T1-weighted magnetic resonance imaging (MRI) of the brain consistent with the known regional brain deposition that occurs with increased Mn exposure (Tuschl et al., 2016).

In the present work, *Slc39a14*-KO mice express motor function deficits and dystonia-like movement with elevated blood and brain Mn concentrations similar to humans carrying the *SLC39A14* mutation (Fig. 1 and Fig. 2). An early onset dystonia was expressed in the form of trunk twisting and hind limb clasping that appeared at PN21 and remained in PN60 *Slc39a14*-KO mice. Importantly, at PN21, some of the *Slc39a14*-KO mice (see Supplementary Movie 1) exhibited backward walking similar to moonwalker mice (Becker et al., 2009). The moonwalker mice are a model of inherited cerebellar ataxia resulting from a gain-of-function mutation in the gene encoding the cation-permeable transient receptor potential channel (TRPC3) (Becker et al., 2009). Further, *Slc39a14*-KO mice expressed torticollis and straub tail as described in previous studies (Aydemir et al., 2017; Xin et al., 2017; Jenkitkasemwong et al., 2018). It has been suggested that these postural abnormalities could affect behavioral performance of the *Slc39a14*-KO mice (Taylor et al., 2020). However, a recent study has shown that *Slc39a14*-KO mice with torticollis and/or straub tail, had deficits in behavioral test scores similar to *Slc39a14*-KO mice that did not display these postural abnormalities (Giraldo and Janus, 2021). Therefore, the postural abnormalities do not interfere with the accurate assessment of motor function deficits in *Slc39a14*-KO mice.

The *Slc39a14*-KO mice used in this study also express deficits in other motor function tests as it was noted in the original manuscript that first described the *Slc39a14*-KO mice used in the present study. In their work, the authors showed significant impairment in the balance beam, pole descent test, and fore limb activity (Aydemir et al., 2017) at a similar age (PN60) and in older (up to PN120) *Slc39a14*-KO mice than in the present study. Other studies assessing the behavioral phenotype of *Slc39a14*-KO mice also showed motor function deficits and postural abnormalities with dystonia-like movements (Xin et al., 2017; Jenkitkasemwong et al., 2018) consistent with our current findings.

The dystonia-parkinsonism resulting from high brain Mn concentrations in human subjects carrying the inherited *SLC39A14* mutation is thought to involve the basal ganglia due to their role in motor function, but until now, no studies have investigated the neurochemical or neuropathological changes responsible for this clinical phenotype. In the present study, we examined the nigrostriatal dopaminergic system

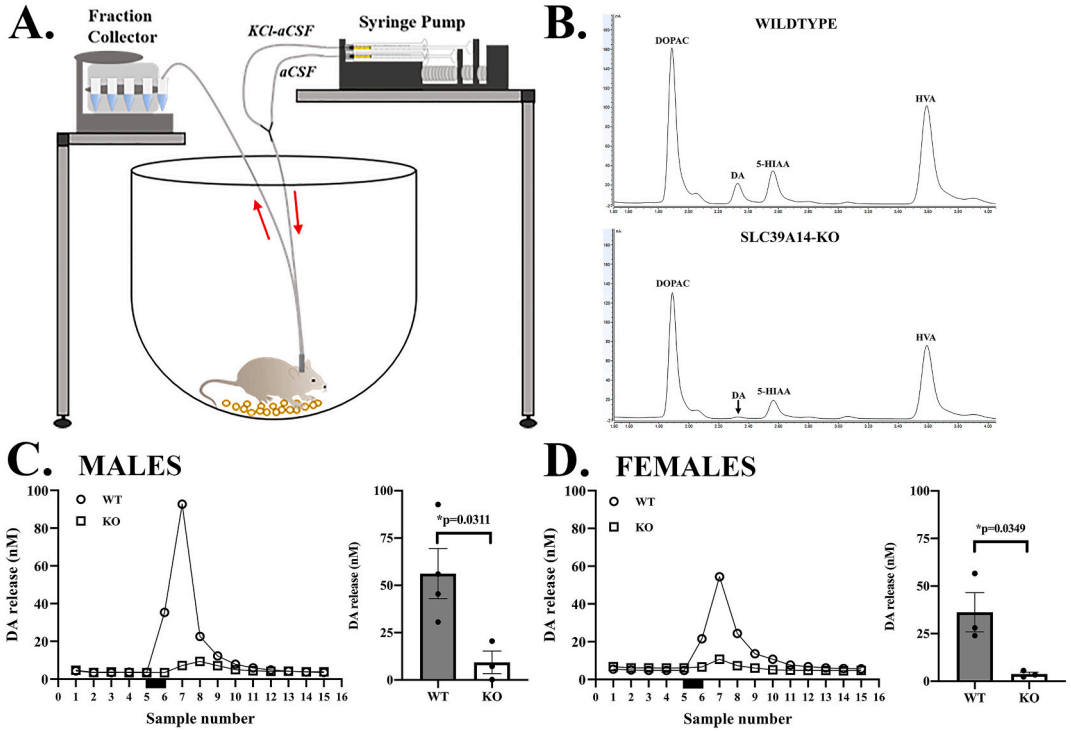

Fig. 5. Analysis of *in vivo* basal and potassium-stimulated dopamine release in the striatum: We performed analysis of brain dialysate DA concentrations using *in vivo* microdialysis to assess extracellular basal and potassium-stimulated DA release in the striatum. For these studies, (A) one WT and *Slc39a14*-KO mice of the same age and sex were paired and microdialysis performed at the same time with the same solution using a T split to perfuse each animal's brain and dialysates from each animal was collected and were immediately analyzed using an HPLC with electrochemical detection. (B) Representative HPLC-electrochemical chromatogram from a WT and *Slc39a14*-KO mice. (C) Representative basal and potassium-stimulated DA levels in dialysates as a function of time in WT and *Slc39a14*-KO male mice. Quantification of results in provided in the graph to the right of DA release graph. (n = 3–4) (D) Representative basal and potassium-stimulated DA levels in dialysates as a function of time in WT and *Slc39a14*-KO female mice. Black bar between sample numbers 5 and 6 was the beginning and ending of potassium infusion. Quantification of results in provided in the graph to the right of DA release graph. (n = 3) Values are mean ± SEM.

because of its important role in motor function. In addition, the main neuropathology in idiopathic Parkinson's disease is the loss of DA, specifically the DA terminals in the striatum and DA cell bodies in the SNc (Guilarte, 2010; Guilarte, 2013; Guilarte and Gonzales, 2015; Blanc, 2018). We found that *Slc39a14*-KO mice had normal levels of striatal DA and metabolites as well as their ratios relative to WT (Fig. 3). Furthermore, analysis of DAergic terminals in the striatum using TH immunohistochemistry did not show any difference between *Slc39a14*-KO and WT mice, and this was supported by unbiased stereological counting of TH-positive and Nissl-stained neurons in the SNc (Fig. 4 and supplementary Fig. 4). The results showed no differences in DA neuron density or soma volume in the SNc of *Slc39a14*-KO mice relative to WT (Fig. 4 and Supplementary Fig. 4). Moreover, the estimated number of TH-positive and Nissl-stained neurons in the SNc did not differ between *Slc39a14*-KO and WT mice (Supplementary Table 2). Finally, *in vivo* microdialysis in the striatum of *Slc39a14*-KO and WT mice performed at the same time in pairs under the same experimental conditions showed a marked inhibition (85–90%) of potassium-stimulated DA release in *Slc39a14*-KO mice (Fig. 5). This finding is consistent with previous studies from our laboratory in which we found marked inhibition of amphetamine-stimulated DA release in the caudate/putamen of non-human primates chronically exposed to Mn using PET (Guilarte et al., 2006; Guilarte et al., 2008) and in Mn-exposed adult mice (Khalid et al., 2011).

The molecular and cellular mechanism(s) of Mn-induced inhibition of DA release is currently not known. However, recent studies using primary neuronal cultures indicate that Mn disrupts SNARE-protein complex vesicle fusion (Wang et al., 2016), an effect that could be mediated via a Mn-induced overexpression of α-synuclein (Wang et al., 2018). These findings indicate that the behavioral phenotype described in *Slc39a14*-KO mice is due, at least in part, to presynaptic function deficits in the form of marked inhibition of DA release with no change in DA or metabolite concentrations in the striatum. Importantly, nigrostriatal DAergic terminals and DA neuron number, density, and soma volume in the SNc were not affected in *Slc39a14*-KO mice relative to WT (Fig. 3, Fig. 4 and Supplementary Fig. 4; Supplementary Table 2). While detailed neuropathological studies of DAergic neurons in the SNc of *SLC39A14* mutation carriers are lacking, a case report of an ephedrone addict has recently been described (Sanotsky et al., 2020). In this case report, they show that the brain of a 33-year-old female ephedrone addict, with increased brain Mn and a history of levodopa unresponsive parkinsonism with dysarthria, dystonia, postural instability, cock-gait, and frequent falls, exhibited normal TH-positive staining in DAergic neurons in the SNc (Sanotsky et al., 2020) consistent with our current results. However, unlike our present study, this case report did not quantify DA neuron number in the SNc.

Our current study provides direct evidence of a dysfunctional but structurally intact nigrostriatal DAergic system in *Slc39a14*-KO mice that exhibited elevated brain Mn concentrations and motor function deficits, dystonia-like movements, and postural abnormalities. This is consistent with the clinical data from Tuschl et al., 2016, indicating that subjects with the inherited *SLC39A14* mutation do not respond to levodopa therapy [supplementary note 1 in 29]. Our present finding of marked inhibition of DA release in the striatum with no change in DA concentrations or DA neuron degeneration is similar to a mouse model of *DYT1* dystonia (Ip et al., n.d.). *DYT1* dystonia or early onset torsion dystonia is the most common form of hereditary primary dystonia caused by a mutation in the *TOR1* gene which codes for the torsin A protein. In this dystonia mouse model, the genetic mutation did not affect striatal DA concentrations but produced a marked inhibition of

amphetamine-induced DA release in the striatum (Balcioglu et al., 2007). Inhibition of DA release in the striatum has also been described in other animal models of dystonia (Balcioglu et al., 2007; Hewett et al., 2010; Fan et al., 2012; Ip et al., n.d.; Eskow Jaunarajs et al., 2019; Rauschenberger et al., 2020).

While it is clear that *Slc39a14*-KO mice expressed marked inhibition of DA release, it is not clear which of the motor function changes, dystonia-like movements, and postural and gait abnormalities are associated with this neurochemical deficit. Future rescue studies are likely to provide an answer to this important question. Although in this communication we found no neurodegeneration of TH-positive DAergic neurons in the SNc, it is possible that neurodegeneration is occurring in other brain regions as suggested in the original Tuschl et al., report (Tuschl et al., 2016). That is, they show evidence of neuronal loss in the globus pallidus and dentate nucleus of the cerebellum as well as cortical and cerebellar atrophy in one *SLC39A14* inherited mutation carrier (Tuschl et al., 2016). As some *Slc39a14*-KO mice at weaning (PN21) exhibited backward walking with spreading of the hind limbs resembling the same deficit in moonwalker mice (Becker et al., 2009), this finding also suggests cerebellar involvement in the pathophysiology of *Slc39a14*-KO mice. Further evidence of cerebellar involvement exists in other genetic animal models of dystonia and in the human disease (Shakkottai et al., 2017; Tewari et al., 2017). Future studies will examine these possibilities in *Slc39a14*-KO mice. While Mn-induced neurological disease was first described nearly two centuries ago (Couper, 1837; Guilarte, 2010; Blanc, 2018), the precise molecular and cellular mechanism(s) and underlying neuropathology are less defined. Therefore, *Slc39a14*-KO mice, as well as *Slc30a10*-KO mice, will facilitate additional discoveries on the pathophysiology of Mn neurotoxicity with significant translational implications for the development of effective therapeutic strategies. Finally, although it is highly likely that the behavioral and neurochemical effects that we observed in the present work are the result of the highly elevated brain Mn concentrations, it is possible that there are Mn-independent effects resulting from the loss of the *Slc39a14* gene. Rescue experiments in which brain Mn accumulation are prevented in *Slc39a14*-KO mice are important to determine whether the loss of *Slc39a14* gene expression has any independent effects on the behavioral or neurochemical changes described in this communication.

Supplementary data to this article can be found online at https://doi.org/10.1016/j.nbd.2021.105467.

Declaration of Competing Interest

The authors declare no competing interest.

Acknowledgements

This work was supported by funding from the Office of Research and Economic Development at Florida International University and National Institute of Environmental Health Sciences (NIEHS) Grant R01-ES029344 to TRG. ANR was supported by National Institutes of Health (NIH) training grant T32-GM13205401 at Florida International University.

References

Aschner, J.L., Aschner, M., 2005. Nutritional aspects of manganese homeostasis. Mol. Asp. Med. 26, 353–362. https://doi.org/10.1016/j.mam.2005.07.003.

Aydemir, T.B., Sitren, H.S., Cousins, R.J., 2012. The zinc transporter ZIP14 influences c-Met phosphorylation and hepatocyte proliferation during liver regeneration in mice. Gastroenterology 142. https://doi.org/10.1053/j.gastro.2012.02.046, 1536–1546. e5.

Aydemir, T.B., et al., 2017. Metal transporter Zip14 (Slc39a14) deletion in mice increases manganese deposition and produces neurotoxic signatures and diminished motor activity. J. Neurosci. 37, 5996–6006. https://doi.org/10.1523/JNEUROSCI.0285-17.2017.

Balcioglu, A., et al., 2007. Dopamine release is impaired in a mouse model of DYT1 dystonia. J. Neurochem. 102, 783–788. https://doi.org/10.1111/j.1471-4159.2007.04590.x.

Becker, E.B.E., et al., 2009. A point mutation in TRPC3 causes abnormal Purkinje cell development and cerebellar ataxia in moonwalker mice. Proc. Nat. Acad. Sci. 106, 6706–6711. https://doi.org/10.1073/pnas.0810599106.

Blanc, P.D., 2018. The early history of manganese and its recognition of its neurotoxicity. NeuroToxicol. 64, 5–11. https://doi.org/10.1016/j.neuro.2017.04.006.

Brna, P., Gordon, K., Dooley, J.M., Price, V., 2011. Manganese toxicity in a child with iron deficiency and polycythemia. J. Child Neurol. 26, 891–894. https://doi.org/10.1177/0883073810393962.

Colosimo, C., Guidi, M., 2009. Parkinsonism due to ephedrone neurotoxicity: a case report. Eur. J. Neurol. 16, e114–e115. https://doi.org/10.1111/j.1468-1331.2009.02606.x.

Couper, J., 1837. On the effects of the black oxide of manganese when inhaled in the lungs. Brit. Ann. Med. Pharmacol. 1, 41–42.

de Bie, R.M., Gladstone, R.M., Strafella, A.P., Ko, J.H., Lang, A.E., 2007. Manganese-induced parkinsonism associated with methcathinone (ephedrone) abuse. Arch. Neurol. 64, 886–889. https://doi.org/10.1001/archneur.64.6.886.

Eskow Jaunarajs, K.L., Scarduzio, M., Ehrlich, M.E., McMahon, L.L., Standaert, D.G., 2019. Diverse mechanisms lead to common dysfunction of striatal cholinergic interneurons in distinct genetic mouse models of dystonia. J. Neurosci. 39, 7195–7205. https://doi.org/10.1523/JNEUROSCI.0407-19.2019.

Song, C.-H., Fan, X., Exeter, C.J., Hess, E.J., Jinnah, H.A., 2012. Functional analysis of dopaminergic systems in a DYT1 knock-in mouse model of dystonia. Neurobiol. Dis. 48, 66–78. https://doi.org/10.1016/j.nbd.2012.05.009.

Fudalej, S., Kolodziejczyk, I., Gajda, T., Majkowska-Zwolinska, B., Wojnar, M., 2013. Manganese-induced parkinsonism among ephedron users and drug policy in Poland. J. Addict. Med. 7, 302–303. https://doi.org/10.1097/ADM.0b013e3182915dce.

Giraldo, G., Janus, C., 2021. Phenotypic evaluation of a childhood-onset parkinsonism-dystonia mouse model with inherent postural abnormalities. Brain Res. Bull. 166, 54–63. https://doi.org/10.1016/j.brainresbull.2020.10.018.

Gospe, S.M., et al., 2000. Paraparesis, hypermanganesaemia, and polycythaemia: a novel presentation of cirrhosis. Arch. Dis. Child. 83, 439–442. https://doi.org/10.1136/adc.83.5.439.

Guilarte, T.R., 2010. Manganese and Parkinson's disease: a critical review and new findings. Environ. Health Perspect. 118, 1071–1080. https://doi.org/10.1590/s1413-81232011001200028.

Guilarte, T.R., 2013. Manganese neurotoxicity: new perspectives from behavioral, neuroimaging and neuropathological studies in humans and non-human primates. Front. Aging Neurosci. 5, 1–10. https://doi.org/10.3389/fnagi.2013.00023.

Guilarte, T.R., Gonzales, K.K., 2015. Manganese-induced parkinsonism is not idiopathic Parkinson's disease: environmental and genetic evidence. Toxicol. Sci. 146, 204–212. https://doi.org/10.1093/toxsci/kfv099.

Guilarte, T.R., et al., 2006. Nigrostriatal dopamine system dysfunction and subtle motor deficits in manganese-exposed non-human primates. Exp. Neurol. 202, 381–390. https://doi.org/10.1016/j.expneurol.2006.06.015.

Guilarte, T.R., et al., 2008. Impairment of nigrostriatal dopamine neurotransmission by manganese is mediated by pre-synaptic mechanism(s): implications to manganese-induced parkinsonism. J. Neurochem. 107, 1236–1247. https://doi.org/10.1111/j.1471-4159.2008.05695.x.

Guilarte, T.R., et al., 2019. PET imaging of dopamine release in the frontal cortex of manganese-exposed non-human primates. J. Neurochem. 150, 188–201. https://doi.org/10.1111/jnc.14681.

Hewett, J., Johanson, P., Sharma, N., Standaert, D., Balcioglu, A., 2010. Function of dopamine transporter is compromised in DYT1 transgenic animal model in vivo. J. Neurochem. 113, 228–235. https://doi.org/10.1111/j.1471-4159.2010.06590.x.

Ip, Chi Wang, et al., 2016. Tor1a+/− mice develop dystonia-like movements via a striatal dopaminergic dysregulation triggered by peripheral nerve injury. Acta Neruopathol. Commun. 4, 108. https://doi.org/10.1186/s40478-016-0375-7.

Iqbal, M., Monaghan, T., Redmond, J., 2012. Manganese toxicity and ephedrone abuse manifesting as parkinsonism: a case report. J. Med. Case Rep. 6, 52. https://doi.org/10.1186/1752-1947-6-52.

Janocha-Litwin, J., Marianska, K., Serafinska, S., Simon, K., 2015. Manganese encephalopathy among ephedron abusers-case reports. J. Neuroimaging 25, 832–835. https://doi.org/10.1111/jon.12173.

Jenkitkasemwong, S., et al., 2018. SLC39A14 deficiency alters manganese homeostasis and excretion resulting in brain manganese accumulation and motor deficits in mice. Proc. Nat. Acad. Sci. 115, E1769–E1778. https://doi.org/10.1073/pnas.1720739115.

Juneja, M., et al., 2018. A novel mutation in SLC39A14 causing hypermanganesemia associated with infantile onset dystonia. J. Genet. Med. 20, e3012 https://doi.org/10.1002/jgm.3012.

Khalid, M., Aoun, A.R., Mathews, A.T., 2011. Altered striatal dopamine release following a sub-acute exposure to manganese. J. Neurosci. Methods 202, 182–191. https://doi.org/10.1016/j.jneumeth.2011.06.019.

Lechpammer, M., et al., 2014. Pathology of inherited manganese transporter deficiency. Ann. Neurol. 75, 608–612. https://doi.org/10.1002/ana.24131.

Liang, C.-C., Tanabe, L.M., Jou, S., Chi, F., Dauer, W.T., 2014. Torsin a hypofunction causes abnormal twisting movements and sensorimotor circuit neurodegeneration. J. Clin. Invest. 124, 3080–3092. https://doi.org/10.1172/JCI72830.

Loth, M.K., et al., 2016. TSPO in a murine model of Sandhoff disease: presymptomatic marker of neurodegeneration and disease pathophysiology. Neurobiol. Dis. 85, 174–186. https://doi.org/10.1016/j.nbd.2015.11.001.

Marti-Sanchez, L., et al., 2018. Hypermanganesemia due to mutations in *SLC39A14*: further insights into Mn deposition in the central nervous system. Orphanet J. Rare Dis. 13, 28. https://doi.org/10.1186/s13023-018-0758-x.

Meral, H., Kutukcu, Y., Atcama, B., Ozer, F., Hamamcioglu, K., 2007. Parkinsonism caused by chronic usage of intravenous potassium permanganate. Neurologist 13, 92–94. https://doi.org/10.1097/01.nrl.0000253089.20746.a8.

Mukhopadhyay, S., 2018. Familial manganese-induced neurotoxicity due to mutations in *SLC30A10* and *SLC39A14*. NeuroToxicol. 64, 278–283. https://doi.org/10.1016/j.neuro.2017.07.030.

Nunes, J.A., et al., 2010. A simple method based on ICP-MS for estimation of background levels of arsenic, cadmium, copper, manganese, nickel, lead, and selenium in blood of the Brazilian population. J. Toxicol. Environ. Health A 73, 878–887. https://doi.org/10.1080/15287391003744807.

Paxinos, G., Franklin, K.B., 2001. The Mouse Brain: In Stereotaxic Coordinates, 2nd edition. Academic Press.

Poniatowska, R., et al., 2014. MRI brain findings in ephedrine encephalopathy associated with manganese abuse: single-center perspective. Pol. J. Radiology 79, 150–155. https://doi.org/10.12659/PJR.889690.

Quadri, M., et al., 2012. Mutations in *SLC30A10* cause parkinsonism and dystonia with hypermanganesemia, polycythemia, and chronic liver disease. Am. J. Hum. Genet. 90, 467–477. https://doi.org/10.1016/j.ajhg.2012.01.017.

Rauschenberger, L., et al., 2020. Striatal dopaminergic dysregulation and dystonia-like movements induced by sensorimotor stress in a pharmacological mouse model of rapid-onset dystonia-parkinsonism. Exp. Neurol. 323, 113109. https://doi.org/10.1016/j.expneurol.2019.113109.

Rodan, L.H., et al., 2018. Novel founder intronic variant in SLC39A14 in two families causing manganism and potential treatment strategies. Mol. Genet. Metab. 124, 161–167. https://doi.org/10.1016/j.ymgme.2018.04.002.

Sahni, V., et al., 2007. Case report: a metabolic disorder presenting a pediatric manganism. Environ. Health Persp. 115, 1776–1779. https://doi.org/10.1289/ehp.10421.

Sanotsky, Y., et al., 2007. Manganic encephalopathy due to “ephedrone” abuse. Mov. Disord. 22, 1337–1343. https://doi.org/10.1002/mds.21378.

Sanotsky, Y., et al., 2020. Neuropathological findings in ephedrone encephalopathy. Mov. Disord. 35, 1858–1863. https://doi.org/10.1002/mds.28125.

Selikhova, M., et al., 2008. Parkinsonism and dystonia caused by illicit use of ephedrone-a longitudinal study. Mov. Disord. 23, 2224–2231. https://doi.org/10.1002/mds.22290.

Shakkottai, V.G., et al., 2017. Current opinions and areas of consensus on the role of the cerebellum in dystonia. Cerebellum 16, 577–594. https://doi.org/10.1007/s12311-016-0825-6.

Sherwood, C.C., Raghanti, M.A., Wenstrup, J.J., 2005. Is humanlike cytoarchitectural asymmetry present in another species with complex social vocalization? A stereologic analysis of mustached bat auditory cortex. Brain Res. 1045, 164–174. https://doi.org/10.1016/j.brainres.2005.03.023.

Sikk, K., et al., 2007. Irreversible motor impairment in young addicts-ephedrone, manganism or both? Acta Neurol. Scand. 115, 385–389. https://doi.org/10.1111/j.1600-0404.2007.00818.x.

Sikk, K., et al., 2010. Clinical, neuroimaging, and neurophysiological features of addicts with manganese-ephedrone exposure. Acta Neurol. Scand. 121, 237–243. https://doi.org/10.1111/j.1600-0404.2009.01189.x.

Sikk, K., et al., 2013. Manganese-induced parkinsonism in methcathinone abusers: biomarkers of exposure and follow-up. Eur. J. Neurol. 20, 915–920. https://doi.org/10.1111/ene.12088.

Slomianka, L., West, M.J., 2005. Estimators of the precision of stereological estimates: an example based on the CA1 pyramidal cell layer of rats. Neuroscience 136, 757–767. https://doi.org/10.1016/j.neuroscience.2005.06.086.

Stamelou, M., et al., 2012. Dystonia with brain manganese accumulation resulting from *SLC30A10* mutations: a new treatable disorder. Mov. Disord. 27, 1317–1322. https://doi.org/10.1002/mds.25138.

Stepens, A., et al., 2008. A parkinsonian syndrome in methcathinone users and the role of manganese. New Engl. J. Med. 358, 1009–1017. https://doi.org/10.1056/NEJMoa072488.

Taylor, C.A., et al., 2020. Maintaining translational relevance in animal models of manganese neurotoxicity. J. Nutrition 150, 1360–1369. https://doi.org/10.1093/jn/nxaa066.

Tewari, A., Fremoni, R., Khodakhash, K., 2017. It’s not just the basal ganglia: cerebellum as a target for dystonia therapeutics. Mov. Disord. 32 https://doi.org/10.1002/mds.27123, 1537-1454.

Tuschl, K., et al., 2008. Hepatic cirrhosis, dystonia, polycythemia, and hypermanganesemia-a new metabolic disorder. J. Inherit. Metab. Dis. 31, 151–163. https://doi.org/10.1007/s10545-008-0813-1.

Tuschl, K., et al., 2012. Syndrome of hepatic cirrhosis, dystonia, polycythemia, and hypermanganesemia caused by mutations in *SLC30A10*, a manganese transporter in man. Am. J. Hum. Genet. 90, 457–466. https://doi.org/10.1016/j.ajhg.2016.07.015.

Tuschl, K., et al., 2016. Mutations in *SLC31A14* disrupt manganese homeostasis and cause childhood-onset parkinsonism-dystonia. Nat. Commun. 7, 11601. https://doi.org/10.1038/ncomms11601.

Wang, C., et al., 2016. Manganese exposure disrupts SNARE-protein complex-mediated vesicle fusion in primary cultured neurons. Env. Toxicol. 32, 705–716. https://doi.org/10.1002/tox.22272.

Wang, C., et al., 2018. Alpha-synuclein and calpains disrupts SNARE-mediated synaptic vesicle fusion during manganese exposure in SH-SY5Y cells. Cells 7, 258. https://doi.org/10.3390/cells7120258.

Xiao, R., et al., 2020. Abnormal cerebellar development is involved in dystonia-like behaviors and motor dysfunction of autistic BTBR mice. Front. Cell Dev. Biol. 8, 231. https://doi.org/10.3389/fcell.2020.00231.

Xin, Y., et al., 2017. Manganese transporter Slc39a14 deficiency revealed its key role in maintaining manganese homeostasis in mice. Cell Disc. 3, 17025. https://doi.org/10.1038/celldisc.2017.25.

Yang, L., Beal, M.F., 2011. Determination of neurotransmitter levels in models of Parkinson’s disease by HPLC-ECD. Methods in Mol. Biol. 793, 401–415. https://doi.org/10.1007/978-1-61779-328-8_27.

Yildirim, E.A., et al., 2009. Chronic manganese intoxication due to methcathinone (ephedron) abuse: a case report. Turk. J. Psychiatry 20, 294–298.

Zeglam, A., Abugrara, A., Kabuka, M., 2019. Autosomal-recessive iron deficiency anemia, dystonia, and hypermanganesemia caused by a new variant mutation of the manganese transporter gene SLC39A14. Acta Neurol. Belg. 119, 379–384. https://doi.org/10.1007/s13760-018-1024-7.